



ANTEC[®] 2021

2021 PROCEEDINGS

COMPARATIVE STUDY OF FILLED AND UNFILLED POLYLACTIC ACID PRODUCED VIA INJECTION MOLDING AND 3D PRINTING

Chethan Savandaiah¹, Bernhard Plank^{2,3}, Julia Maurer², Juergen Lesslhumer¹, Georg Steinbichler⁴

¹Kompetenzzentrum Holz GmbH, Linz, Austria

²Research Group Computed Tomography, University of Applied Science Upper Austria, Wels, Austria

³Institute of Materials Resource Management, University of Augsburg, Germany

⁴Institute of Polymer Injection Molding and Process Automation, Johannes Kepler University, Linz, Austria

Correspondence: chethan.savand@outlook.com

Abstract

This study investigates the impact of two different processing methods, Injection molding (IM) and 3D printing (3Dp), on neat/unfilled polylactic acid (NPLA) and the short carbon fibers (SCFs) filled polylactic acid (SPLA). Furthermore, the resulting processing conditions and the influence on mechanical properties, such as tensile, flexural, notched Charpy impact test, and heat deflection temperature (HDT), along with the process-induced effects, such as fiber length distribution and voids, were studied. The process-induced voids were evident in all the computed tomography (CT) scans, 3Dp specimens have higher void volume fraction compared to no visible voids in IM specimens. Similarly, the mechanical test results such as tensile, flexural and notched Charpy impact test follow the trend for 3Dp SPLA and IM SPLA. On the contrary, 3Dp 0° and ±45° NPLA tensile test results are comparable to IM NPLA, whereas 3Dp 0° NPLA has the highest impact resistance compared to injection molded NPLA and SPLA as well as 3Dp SPLA specimens, indicating the annealing effect induced by the heated 3D printing bed along with increased void volume fraction. Furthermore, the HDT study indicates the maximum serviceable temperature of both NPLA and SPLA remained comparable regardless of the processing method. Moreover, the change in fiber length distribution for SPLA injection molded and extruded filament specimens were negligible.

Introduction

The advent of low cost open-sourced material extrusion-based 3D printers has catapulted the research and is setting the stage to take over conventional mass-production processing techniques such as injection molding. The advantages of 3Dp over IM, are as follows,

1. Able to produce parts with highly anisotropic material properties [1, 2, 3]
2. Open-sourced 3Dp machines and slicing software [4, 5]

3. No need to develop new tooling/low-cost tooling to produce complex design and can be used in combination with IM [6]
4. No need to develop new materials, pre-existing extrusion grade materials data can be utilized to modify the properties based on the end application [4]
5. Low material wastage [4, 7].

Furthermore, the main attributes of 3Dp parts that need to be addressed are the poor mechanical strength, limited by the polymeric matrix and the poor adhesion between adjacent layers during deposition, and the inherent voids of 3Dp parts. To address this discrepancy, Striemann et al. [4] have systematically studied the influence of processing method, IM and 3Dp, on PA-6 reinforced with SCF and subsequently investigated the processing-induced defects and its influence on mechanical properties. Also, Boros et al. [6] have discussed a novel approach of combining two processing technologies, IM and 3Dp, to address the complex design and to overcome processing constraints with help of 3Dp. The authors have studied the effect and influence of over-molding and over-printing of PLA material and reported the successful joining of 3Dp part with over-molding and vice versa. Furthermore, Sanders et al. [5], comparatively studied the mechanical properties of impact-modified polypropylene-copolymer parts produced via IM and 3Dp, similar to earlier reports, parts produced via 3Dp underperformed, with a loss of 30% in mechanical strength compared to IM parts. Furthermore, the authors have applied the post-processing technique for 3Dp parts, such as the part consolidation method, and reported significant improvement in mechanical strength as compared to IM parts. The post-consolidation technique would be beneficial for producing parts with highly anisotropic material properties with no voids.

The goal of this paper is to provide additional material data sets to the limited research output with regards to the comparative study of PLA and PLA filled with SCF in IM and 3Dp processing techniques. In this paper, authors have performed standardized tests and

evaluated the data sets accordingly for both IM and 3Dp specimens. The tests include tensile tests, notched Charpy Impact tests, three-point bending tests, and HDT. To understand the process-induced effects, the authors have utilized fiber length distribution and CT scans analysis.

Materials and Methods

A PLA homopolymer (density 1.24 g/cm³, melting temperature 175°C) with high viscosity, suitable for film extrusion, thermoforming, or fiber spinning was purchased from Total Corbion. The particulate carbon fiber without sizing, Tenax HT (diameter 7 μm, fiber length 60–80 μm and density 1.82 g/cm³) was purchased from Teijin, USA.

The binding matrix formulation was prepared in the Brabender twin-screw extruder 20/40 D, and the material loading was done via gravimetric dosing units. The 6 heating zones temperature was maintained between 200–220°C. The melt mixing was carried out at 375 rpm, while the melt temperature was maintained at 215°C. Initially, PLA (7.5 wt.%) is melted in the melting zone and is followed by the addition of SCF (25 wt.%) in the mixing zone to produce filled composite (SPLA). The homogenized composite material was then granulated with help of an underwater granulation system.

The filament extrusion was carried out for NPLA and SPLA in Brabender conical twin-screw extruder Mark III, and the material feeding was done via gravimetric dosing unit. The 6 heating zones were operated between 195–215°C, while the melt temperature was maintained at 210°C. The extrusion speed was regulated by the melt pump, while the filament extrusion rate was maintained at 20 cm³/min. The extruded filament was passed through an air-cooled haul off system to maintain the winding temperature near to atmospheric temperature. Meanwhile, the fiber diameter was constantly monitored and maintained to the industry standard of 1.75 ± 0.05 mm with the help of the BETA LaserMike ovality measurement device along with AccuNet, supplied by NDC GmbH, Germany.

An IM system (SmartPower 120/350_Unilog B8, Wittmann-Battenfeld, Austria) is utilized to produce EN ISO 527-2:2012 1A dimension specimens and the parameters are shown in Table 1. Test IM specimens for impact, flexural and heat deflection temperature testing were produced by cutting off the shoulders from the dog-bone shaped tensile test specimens using a MUTRONIC Diadisc 4200 precision cut-off saw. A 2 mm V notch specimen was also created with the same machine. The samples were stored in control room for 72 h.

The 3Dp sample were prepared on open source Prusa I3 MK3S printer manufactured by Prusa Research, Czech

Republic, and the instructions for 3D printing were prepared in a slicing software, Simplify 3D (ver. 4.0.1) with different printing raster configuration. The process settings are summarized in Table 2, such as temperature, layer height, speed to flow ratio, bed temperature, which were standardized for all the test specimens. The print bed and printed samples were cooled down to nominal room temperature to avoid part distortion/warping and facilitate ease of removal. Furthermore, before testing, the removed samples were stocked in the standard control room for 72 h.

Table 1. Selected IM parameters.

| Parameters | Unit | NPLA | SPLA |
|-----------------------|--------------------|------|------|
| Dosage volume | cm ³ | 45 | 45 |
| Screw temperature | °C | 195 | 195 |
| Injection flow | cm ³ /s | 50 | 50 |
| Residual cooling time | s | 46 | 14 |
| Injection pressure | MPa | 72 | 152 |
| Backpressure | MPa | 50 | 5 |

Table 2. Important 3Dp process settings, where NA = Not applicable

| Parameters | Unit | Values |
|-------------------------------|------|----------------|
| Nozzle temperature | °C | 215 |
| Plastic flow multiplier | NA | 0.95 |
| layer height | mm | 0.1 |
| Nozzle diameter | mm | 0.4 |
| Nozzle material | NA | Hardened steel |
| Bed temperature | °C | 85 |
| TP perimeter count | NA | 1 |
| Infill angle (XY orientation) | NA | 0° and ±45° |
| Print speed | mm/s | 55 |
| Infill | % | 100 |

To measure the fiber length of the IM and extruded specimen, the matrix was first removed by pyrolysis in a GERO HTK8 chamber furnace at 500°C for 1 h in the N₂ atmosphere. The recovered fibers were suspended in water, and the fiber length distribution (FLD) was determined using a FASEP 3E-ECO system. Two pictures of each sample were analyzed. Depending on the average fiber length, the number of measured fibers varied between 11,000 and 42,000.

The tensile tests were carried out following EN ISO 527-2:2012 1A dimension. A universal testing machine (UTM) MESSPHYSIK BETA 20–10/4 × 11 equipped with a 10 kN load cell and a video extensometer for strain measurement were used to perform the tests. The modulus of elasticity was determined at a test speed of 1 mm/min and tensile strength at 50 mm/min.

Test specimens prepared for three-point bending tests were following EN ISO 178 standard dimension, and the measurements were performed with UTM equipment, MESSPHYSIK BETA 50. A total of five specimens of each sample type were measured and was carried out at 2 mm/min test speed. The obtained results were evaluated at a significance level of 5%.

The printed specimens were prepared according to EN ISO 179-1 (1/e/A) standard dimension, where a wedge-shaped cutting blade with a notch depth of 2 mm and a tip radius of 0.25 mm was used to create a notch on the individual specimen. Instron CEAST 9050 Impactor II equipped with 0.5 J pendulum and 2 J pendulum (only for 3Dp 0°-NPLA, energy absorbed was higher than 90% of 0.5 J pendulum) was used given that the absorbed energy was well within the range of 10–90% of the selected pendulum energy. In total, 10 specimens for each sample were measured and impact tested. The results were evaluated at a significance level of 5%.

To quantify the void content as well as inclusions of higher density, X-ray computed tomography (CT) scans were performed on a Nanotom 180NF (GE phoenix X-ray, Germany) laboratory CT device. To get an overview of a larger sample volume and to reduce measurement time, an initial scan of all six samples at once was conducted with a voxel size of $(13 \mu\text{m})^3$. Additional, high-resolution CT scans at $(6.5 \mu\text{m})^3$, $(2.75 \mu\text{m})^3$, and $(1.25 \mu\text{m})^3$ were performed on the 3Dp specimens to get reliable quantitative values regarding the void content. High-resolution scans are used as a reference for porosity evaluations to fit the ‘ISO-X’ threshold procedure mentioned by Plank et al. [8] and Senck et al. [9]. This method is also suitable for 3D printed parts as already shown in [10]. To reach a resolution of $(1.25 \mu\text{m})^3$ a small sample with a size of $2 \times 2 \times 10 \text{ mm}^3$ was milled out of the notched Charpy impact tested specimen 3Dp SPLA 45°.

CT data were subsequently analyzed with the porosity/inclusion analysis tool by VGstudio MAX 3.2 (Volume Graphics GmbH, Germany). The defect and porosity analysis is based on the gray value distribution. To evaluate the CT scans performed at $(6.5 \mu\text{m})^3$ voxel size, an ISO-50 threshold (grey value at 50 % between background and material peak) was used for the large voids present in the NPLA specimens, and an ISO-46 threshold was determined as the proper threshold for the small voids present in the SPLA specimens.

Results and Discussion

The fiber retention length and the length distribution within the polymer matrix are highly dependent on fiber's loading volume and processing methods [11]. Specifically, the fiber loading volume, fiber retention lengths, and orientation are the determining factors for the

reinforced polymer's strength. The weight average value of IM and extruded filament is comparable to that of the original length (see Materials and Methods). In Figure 1, the trivial difference in fiber length after processing, IM and extrusion, samples indicate the fiber did not undergo a further reduction in length, as the starting length of the carbon fibers was very short. Both IM and extruded samples retained the fiber length within the starting fiber length range (indicated with arrows).

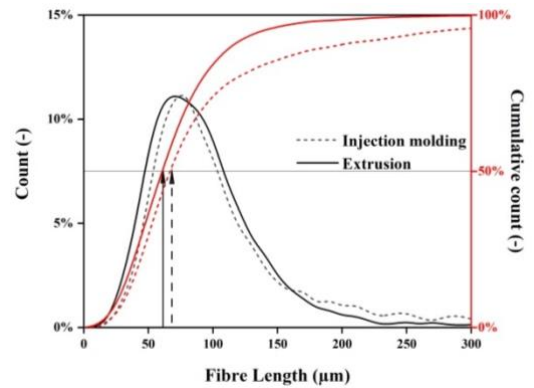


Figure 1. Fiber length distribution of Injection molded specimen and extruded filament.

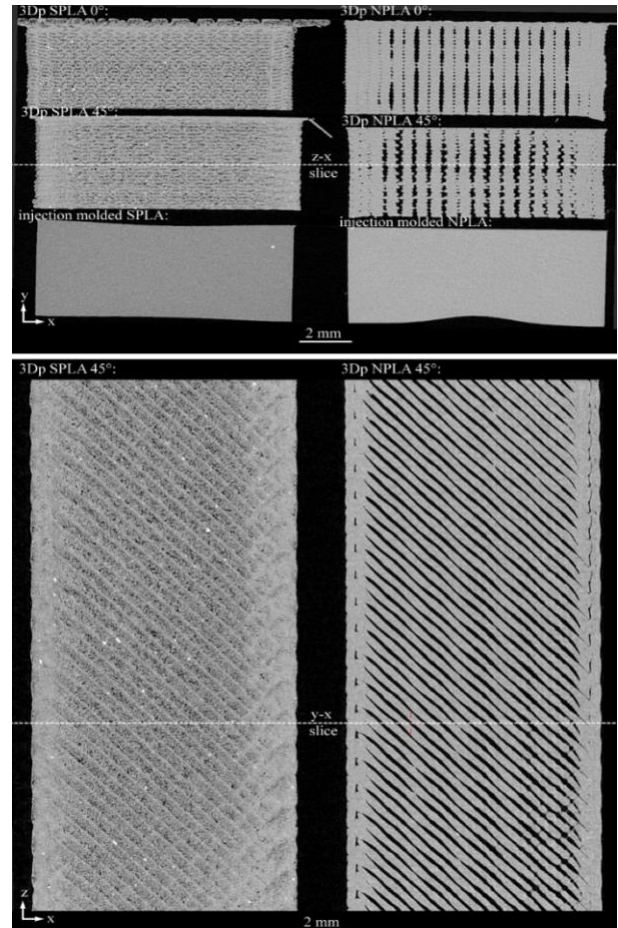


Figure 2. Slices acquired at $(13\ \mu\text{m})^3$ voxel size showing all six specimens in axial x-y slices (top). The frontal x-z slices showing the $\pm 45^\circ$ SPLA and $\pm 45^\circ$ NPLA specimens (bottom).

Figure 2 shows the initial results gained by CT. At $(13\ \mu\text{m})^3$ voxel size all six specimens could be investigated at once, showing already big differences regarding void distribution (dark grey values) and higher-density inclusions (bright grey values). The 3Dp NPLA specimens contain very large voids compared to the small voids in the 3Dp SPLA specimens, which are hardly visible at this voxel resolution. In the injection-molded specimens (bottom row of the x-y slice view) no voids were visible. Higher-density inclusions could mainly be observed in the SPLA specimens (left column) of the axial x-y slices. Looking at the frontal x-z slices, the built direction of the 3Dp 45° samples could be observed.

Figure 3 shows an example of CT results of the NPLA 45° specimen scanned at $(6.5\ \mu\text{m})^3$ voxel size as well the corresponding segmentation with an ISO-50 threshold. As a result, an overall void content of 15.64 vol.% was estimated for this specimen. All voids labeled in red color are connected to a larger void network.

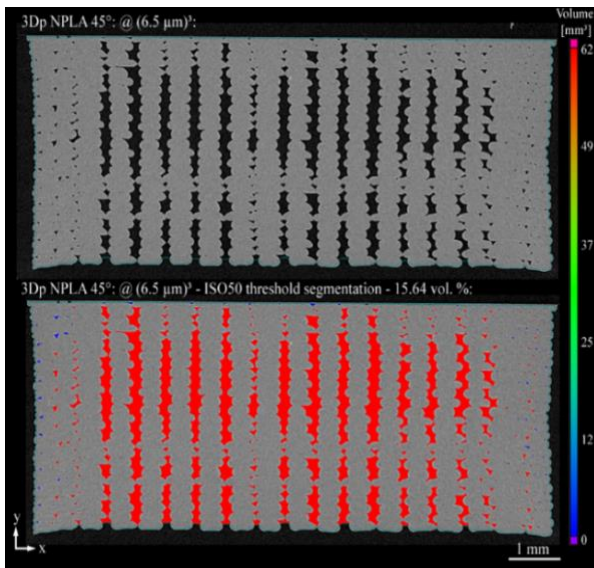


Figure 3. Axial CT slices of the NPLA 45° specimen scanned at $(6.5\ \mu\text{m})^3$ voxel size.

In Figure 4 (top) examples of CT results of the 3Dp SPLA 45° specimen scanned at $(6.5\ \mu\text{m})^3$ voxel size as well the corresponding segmentation with an ISO-46 threshold are shown. This ISO-46 threshold was determined iteratively by using high resolution scans of a small volume and a semi-automated multistep segmentation method for estimating a reference void content [9].

To evaluate the segmentation (labeled in yellow/orange), a region of interest (ROI) is shown in detail and is compared to an high resolution scan performed at $(1.25\ \mu\text{m})^3$ voxel size (Figure 4 bottom). The resulting void content of the ROIs was ~ 16.5 vol.%. In addition at the high resolution scan the individual carbon fibers could be resolved (right). By applying the ISO-46 threshold to the entire 3Dp SPLA 45° CT volume, an overall void content of 13.13 vol.% could be determined.

All quantitative results regarding void content and higher-density inclusions are summarized in Table 3. The 3Dp specimens show very similar void content between 12.21 and 15.9 vol.%. The number of voids per mm^3 and therefore the void size distribution is completely different ranging from 5007 $1/\text{mm}^3$ for the 3Dp SPLA 0° specimen to only 5 $1/\text{mm}^3$ for the 3Dp NPLA 45° specimen. Qualitatively, these results were already revealed in Figures 2-4. Visual results discussing the amount of higher-density inclusions in Figure 2 can also be approved by evaluating the inclusion content. In the 3Dp SPLA specimens, more higher-density inclusions are present.

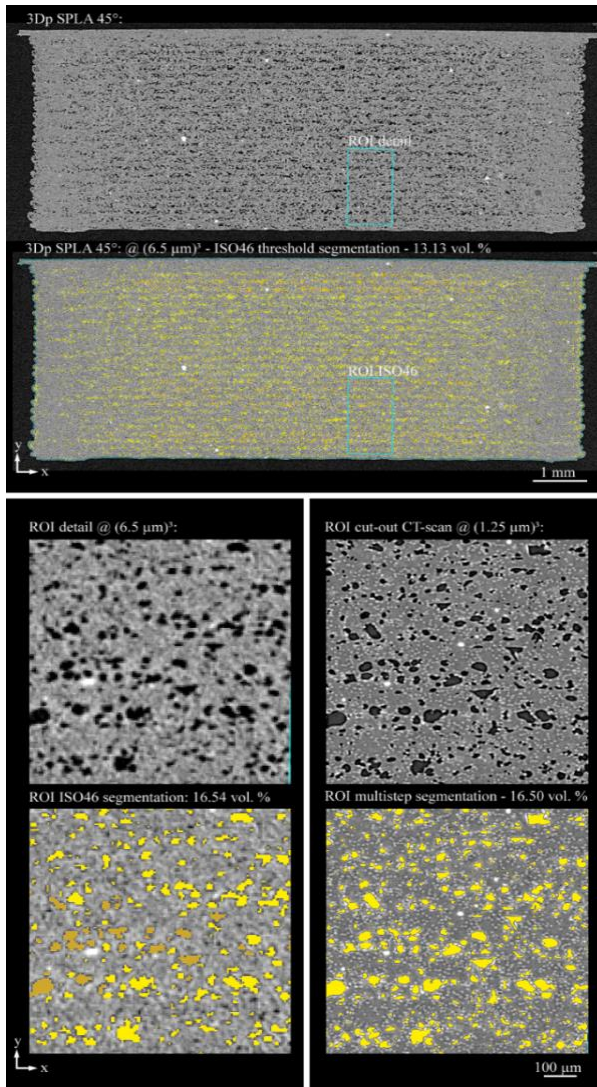


Figure 4. Axial CT slices of the SPLA 45° specimen scanned at $(6.5 \mu\text{m})^3$ (top) and detailed view on the microstructure visible in the region of interest (ROI) additionally scanned at $(1.25 \mu\text{m})^3$ voxel size (bottom).

Table 3. CT results summarizing content of voids and higher-density inclusions as volume fraction and void count.

| | Void content | | Inclusion content | |
|----------|------------------|--------------------------|-------------------|--------------------------|
| | [vol.%] | [count/mm ³] | [vol.%] | [count/mm ³] |
| SPLA 0° | 15.9 | 5007 | 0.091 | 5.76 |
| SPLA 45° | 13.13 | 3881 | 0.122 | 8.55 |
| NPLA 0° | 12.21 | 12 | 0.000 | 0.02 |
| NPLA 45° | 15.64 | 5 | 0.000 | 0.04 |
| IM- SPLA | No visible voids | | 0.003 | 0.30 |
| IM- NPLA | | | 0.001 | 0.01 |

In Figure 5 3D visualizations of the small micro voids in the 3Dp SPLA 45° specimen (left) with a lot of small separated voids (blue) and some connected void networks

(cyan and red), as well the larger macro void network (red and green) within the 3Dp NPLA 45° specimen (right) are shown.

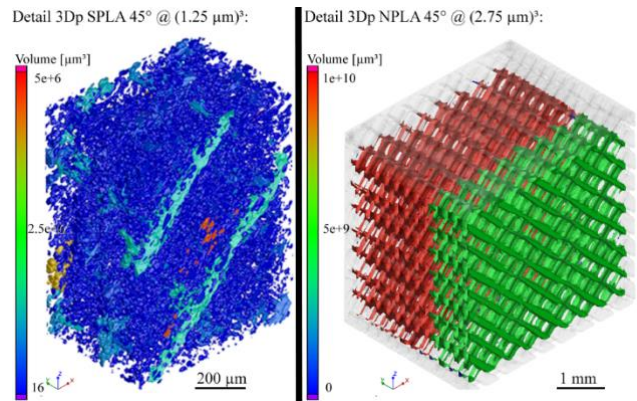


Figure 5. 3D visualization of the small micro voids in the 3Dp SPLA 45° specimen (left) as well the larger macro void network (red and green) within the 3Dpa NPLA 45° specimen (right)

Unterweger et al. [12] and Phua et al. [13] reported HDT increasing with increasing fiber loading and fiber length. However, the HDT results indicate the fibers with length lower than 100 μm do not have a positive influence. Similarly, the trivial difference in HDT, as shown in Table 4, observed for both processing techniques and NPLA and SPLA, indicates that polymer matrix is dominant. Unlike long carbon fiber reinforced polymers, the very short carbon does not influence in restricting the polymer chains movement. For both 3Dp materials, NPLA and SPLA, with raster angle 0° and ±45°, it seems that high void fraction do not influence the HDT.

In Figure 6, in contrast to HDT, the ultimate tensile strength and Young's modulus for IM and 3Dp samples show a major difference between NPLA and SPLA. The short carbon fiber-filled system improved modulus for both IM and 3Dp samples [14]. The ultimate tensile strength seems to favor both IM-NPLA and 3Dp 0° and ±45° NPLA compared to 0° and ±45° SPLA. The IM-SPLA samples show an increase in tensile strength and Young's modulus, by a factor of 1.5 and 3.5, respectively, when compared to IM-NPLA samples.

Table 4. Heat deflection temperature.

| Method | Process | NPLA (°C) | SPLA (°C) |
|----------------------------------|-----------|--------------|--------------|
| HDT- A @ 1.8 MPa- 120°C | IM | 58.4 ± 0.1 | 58.57 ± 0.21 |
| | 3Dp- 0° | 54.6 ± 0.2 | 56.78 ± 0.2 |
| | 3Dp- ±45° | 54.43 ± 0.15 | 59.73 ± 0.1 |

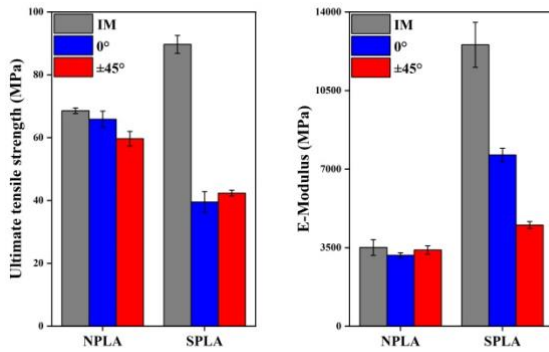


Figure 6. Tensile strength and Young's modulus results of injection molded (IM) and 3Dp (0° and ±45°) specimens

Furthermore, the difference in tensile strength and modulus between IM-NPLA and 3Dp 0° and ±45° NPLA, indicates the effect of annealing similarly reported by Benwood et al., [15] (due to higher bed temperature, see Table 2). Furthermore, the homogenized IM-SPLA shows an increase in strength and modulus by a factor of 1.6 compared to 3Dp 0°-SPLA, the foremost reason is the influence of high void volume fraction with large number of micro voids and hence high void count (see Table 3). The poor layer bonding between the adjacent layers creates inadequate load transfer between the layers.

Figure 7 presents the flexural modulus and strength of IM and 3Dp NPLA and SPLA. IM-NPLA and 3Dp 0°-NPLA have insignificant differences in flexural strength and modulus, whereas IM-SPLA has higher strength and modulus than 3Dp 0°-SPLA, similarly observed in tensile tests. Between 3Dp 0°-SPLA and ±45° SPLA, the 0° has a better reinforcing ability, resulting in highly anisotropic material properties was also reported by Spoerk et al. [1], due to the fibers being oriented along the printing path, resulting in reinforcing the layers to withstand loads. Moreover, the flexural strength and modulus of 3Dp 0°-NPLA are higher compared to ± 45° NPLA even though both samples have similar void volume fraction with large macro voids and hence low void count. This was also observed by Savandaiah et al. [2] and reported this is due to better load bearing ability of 0° raster angle when compared to ±45° raster angle.

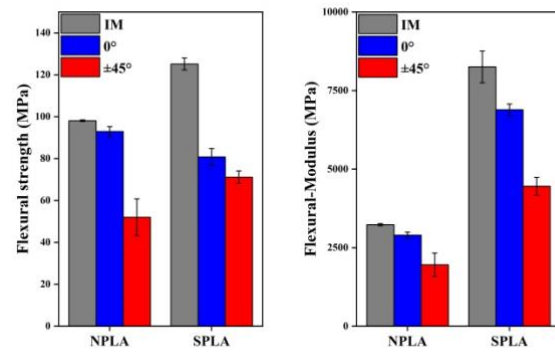


Figure 7. Flexural strength and flexural modulus results of injection molded (IM) and 3Dp (0° and ±45°) specimens

Figure 8 shows notched impact tested results of IM and 3Dp, NPLA and SPLA. Contrary to the results of the other mechanical tests, IM-NPLA ($2.589 \pm 0.142 \text{ kJ/m}^2$) and IM-SPLA ($3.227 \pm 0.348 \text{ kJ/m}^2$) showed similar impact energy, indicating that the impact response is matrix dominant and since the carbon fibers are very short, the load transfer between the matrix and fibers was insufficient. Similarly, 3Dp ±45° NPLA ($2.943 \pm 0.233 \text{ kJ/m}^2$), 3Dp 0°-SPLA ($2.851 \pm 0.087 \text{ kJ/m}^2$), and 3Dp ±45° SPLA ($2.599 \pm 0.125 \text{ kJ/m}^2$) showed similar impact energy. The major outlier, 3Dp 0°-NPLA, has the highest impact resistance ($15.81 \pm 1.55 \text{ kJ/m}^2$).

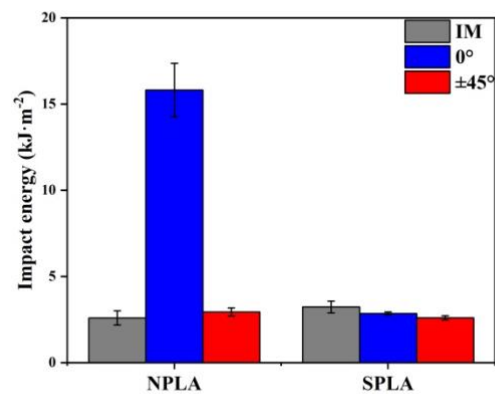


Figure 8. Notched Charpy impact test results of injection molded (IM) and 3Dp (0° and ±45°) specimens

Figure 9 shows different fractures, such as delamination and improper crack propagation, indicating the failure occurrence between the adjacent layers, thereby deflecting and dissipating high impact energy absorbed during the test for the 3Dp 0°-NPLA.

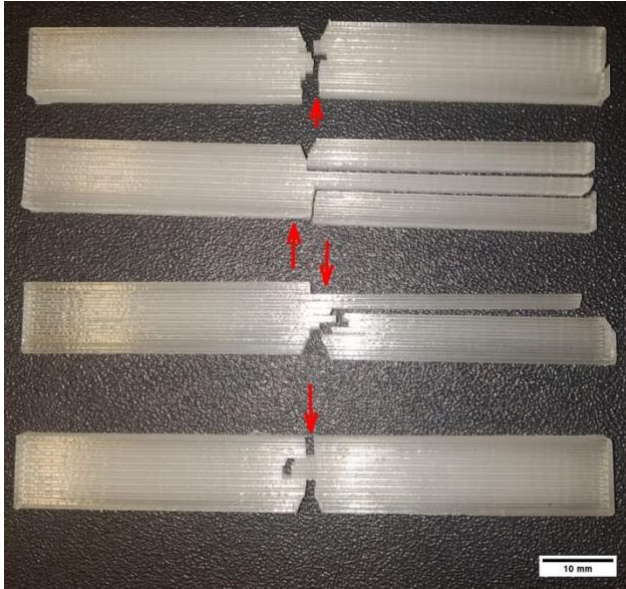


Figure 9. Photography of notched Charpy impact test specimens 3Dp 0°-NPLA, where arrows indicate point impact or direction of impact

Conclusions

In summary, this study demonstrates the importance of a comparative study between injection molding and 3D printing and its processing effect on specimens. The fiber length distribution analysis revealed that fiber length below 100 μm do not undergo process-induced fiber breakage and remain unchanged between 70 μm and 80 μm for extruded filament and IM, respectively. Even though HDT has been shown in the literature to increase with increasing fiber loading and fiber length, the very short carbon fibers did not effectively reinforce the PLA matrix, thereby showing only a mediocre increase in HDT. Furthermore, the CT scan revealed a large cross-sectional area of 3Dp parts were having process-induced voids in the range of 12-16 vol.%, resulting in poor mechanical test performance compared to IM samples. Moreover, the IM-NPLA and 3Dp 0°-NPLA have comparable mechanical test results due to high bed temperature causing an annealing effect even though the void volume fraction was at par with 3Dp SPLA specimens. This was evident in the notched Charpy impact study, for 3Dp 0°-NPLA an increase in impact resistance by a factor of 5 was observed compared to both IM and 3Dp SPLA. The future work would require further investigation on the process control of 3Dp specimens to achieve better mechanical strengths and reduce inherent voids. Further investigations should also be carried out into impact resistance of NPLA relating to the induced annealing effect due to the heated print bed at different temperatures.

Acknowledgment

This research work has been performed as part of the “3D-CFRP” and “Pore3D” (project number: 868735) and “BeyondInspection” (project number: 874540) projects. The authors acknowledge the financial support by the EU funded network M-Era.Net, the BMVIT (Austrian Ministry for Transport, Innovation, and Technology), the FFG (Austrian Research Promotion Agency), the state government of Upper Austria, as well as the RCL (Research Council of Lithuania) and FASIE (Foundation for Assistance to Small Innovative Enterprises, Russia).

Authors express gratitude to Martin Reif and Romana Welser of Kompetenzzentrum Holz GmbH for the sample preparation.

References

1. M. Spoerk, C. Savandaiah, F. Arbeiter, G. Traxler, L. Cardon, C. Holzer, J. Sapkota, *Composites Part-A* (2018).
2. C. Savandaiah, J. Maurer, M. Gall, A. Haider, G. Steinbichler, J. Sapkota, *Journal of Applied Polymer Science* (2020).
3. C. Savandaiah, J. Maurer, J. Lesslhuber, A. Haider, G. Steinbichler. *SPE - ANTEC®: Virtual Edition – 2020*, (2020).
4. P. Striemann, D. Huelsbusch, S. Mrzljak, M. Niedermeier, F. Walther, *Materials Testing*, **62-6**, 567 (2020).
5. J. E. Sanders, L. Wang and D. J. Gardner, *Rapid Prototyping Journal*, **26-6**, 567 (2020).
6. R. Boros, P. Kannan Rajamani, J. G. Kovács, *eXPRESS Polymer Letters*, **13-10**, 897 (2019)
7. E. V. de Toro, J. C. Sobrino, A. M. Martínez, V. M. Eguía and J. A. Pérez, *Materials*, **13**, 672 (2020).
8. B. Plank, G. Rao, and J. Kastner, *Proceedings in 7th International Symposium on NDT in Aerospace*, **10** (2015).
9. S. Senck, M. Scheerer, V. Revol, K. Dobes, B. Plank, and J. Kastner, *AIAA SciTech Forum: 58th AIAA/ASCE/AHS/ASC Structures, Struct. Dyn., Mater. Conf.* (2017).
10. A. Khudiakova, M. Berer, S. Niedermair, B. Plank, E. Truskiewicz, G. Meier, H. Stepanovsky, M. Wolfahrt, G. Pinter, and J. Lackner *Additive Manufacturing*, **14** (2020).
11. T. Wu, Z.-x. Huang, D.-z. Wang, J.-p. Qu, *Advanced Industrial and Engineering Polymer Research*, **2**, 101 (2019).
12. C. Unterweger, T. Mayrhofer, F. Piana, J. Duchoslav, D. Stifter, C. Poitzsch, C. Fürst, *Composite Science and Technology*, **188** (2020).
13. Y.J. Phua, Z.A. Mohd Ishak, R. Senawi, *Journal of Reinforced Plastics and Composites*, **29** (2010).

14. M. Ivey, G. W. Melenka, J. P. Carey, C. Ayranci, *Advanced Manufacturing: Polymer and Composites Sciences*, **3:3**, 91 (2016).
15. C. Benwood, A. Anstey, J. Andrzejewski, M. Misra, and A. K. Mohanty, *ACS Omega*, **3-4**, 4411 (2018).